2014 IEEE International Conference on Robotics & Automation (ICRA)
Hong Kong Convention and Exhibition Center
May 31 - June 7, 2014. Hong Kong, China

Design and Testing of a Novel XY Micropositioning Stage with Dual Ranges and Resolutions

Qingsong Xu, *Member, IEEE*

***Abstract*— This paper presents the design, analysis, and testing of a novel dual-range, dual-resolution XY micropositioning stage driven by a single actuator in each axis. As compared with dual-servo stages, it allows the reduction on the cost of both hardware and control design workload. The compliant stage is devised using leaf springs to achieve a large stroke. Strain sensors are employed to provide coarse and fine resolutions in the larger and smaller motion ranges, respectively. Analytical models are developed to facilitate the quantitative design of the motion ranges and coarse/fine resolution ratio. The motor selection criteria in terms of driving force and stroke are addressed as well. The models are verified through simulations with finite element analysis. A proof-of-concept prototype is fabricated for experimental investigations. The feasibility of the proposed idea is validated by a collection of experimental studies.**

I. Introduction

Micro-/nanopositioning stage is a key device in precision manipulation and assembly systems. Positioning resolution and range are two fundamental performances for a micro-/nanopositioning system. Owing to the limitation of sensor's capability, a higher positioning resolution is usually achieved in a smaller motion range while a larger range is generated with a lower resolution. In practice, many applications demand a micropositioning stage with both a large range and a high resolution for executing diverse tasks. To cater for such requirement, a dual-range positioning stage offers a promising solution.

Conventionally, the dual-servo stage is employed to generate a micropositioning stage with dual ranges and resolutions based on dual actuation. Such a dual-stage consists of a coarse stage and a fine stage, where the latter is mounted on or nested in the former. While the coarse stage provides a large motion range with coarse resolution, the fine stage offers a smaller range with fine resolution. For instance, dual-servo stages using different actuation principles (e.g., piezoelectric, electromagnetic) have been developed in the literature [1]–[5]. In particular, flexure-based compliant stages have been intensively investigated owing to their advantages in terms of no backlash, no friction, and vacuum compatibility [6]–[9].

However, the major issue of a dual-servo stage arises from the interference which is caused by the interaction between the coarse and fine stages. It has been shown that the interaction behavior of a dual-servo stage can lead to an unstable open-loop control system [10]. To attenuate the unwanted interference, the approaches of mechanical design and control design have been developed in the literature. For instance, the interaction effect can be minimized by resorting to an appropriate mechanical design [7]. In addition, the interference may be alleviated by constructing a multiple-input-multiple-output (MIMO) control system based on an interference analysis [11], [12]. Even so, the employment of two type of actuators complicates the mechanism design as well as control design procedures.

The motivation of this paper is to devise a novel dual-range and dual-resolution micropositioning stage using a single drive in each working axis. Specifically, the conceptual design of a compliant stage with dual ranges and resolutions is proposed based on a variable-stiffness compliant mechanism. The mechanism is designed to exhibit different stiffnesses in the small and large ranges, which are enabled by leaf flexures experiencing different magnitudes of bending deformations. The large and small deformations are measured using resistive strain sensors to offer fine and coarse resolutions, respectively. Rather than a dual-servo stage, the presented technique allows the generation of a dual-range positioning by resorting to a single actuator for each working axis. The single-drive design eliminates the conventional interference effect. Furthermore, it renders reduction on hardware cost and stage design workload. The proof-of-concept design is confirmed by both simulation and experimental investigations. The proposed dual-range stage has potential applications in precision positioning situations, e.g., the scenarios which require a fine alignment and a coarse positioning in the smaller and larger ranges, respectively.

The remainder of the paper is organized as follows. The conceptual design of the dual-range, dual-resolution stage is presented in Section II. The mechanical design of a flexure-based XY compliant stage is outlined in Section III. Section IV reports a case study along with performance evaluation of an XY stage through both analytical modeling and finite element analysis (FEA) simulations. A fabricated prototype stage is shown in Section V, where experimental studies are carried out. Section VI summarizes this paper.

II. Conceptual Design of a Dual-Range, Dual-Resolution Stage

A. Dual-Range Compliant Stage Design

The schematic of a single-axis, dual-range micropositioning stage is depicted in Fig. 1. The output platform M is

This work was supported in part by the Macao Science and Technology Development Fund under Grant 070/2012/A3 and in part by the Research Committee of the University of Macau under Grants MYRG083(Y1-L2)-FST12-XQS and MYRG078(Y1-L2)-FST13-XQS.

The author is with the Department of Electromechanical Engineering, Faculty of Science and Technology, University of Macau, Av. Padre Tomás Pereira, Taipa, Macao, China qsxu@umac.mo

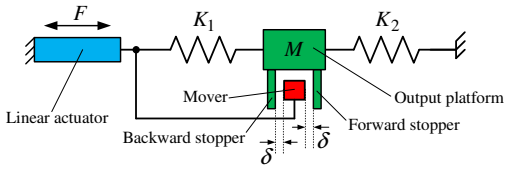

Fig. 1. Illustration of a micropositioning stage with dual-range.

driven by a linear actuator through a compliant bearing with stiffness K_1. In addition, the platform M is fixed through another compliant bearing with stiffness K_2. To obtain two motion ranges for the platform M, a mover is connected to the driving end of the actuator. The translation of the mover is restricted by two stoppers which are mounted on the output platform.

Once the actuator drives the platform M to translate forward (see Fig. 1), both bearings K_1 and K_2 will be compressed. The overall stiffness can be derived as:

$$K_{\text{range1}} = \left(\frac{1}{K_1} + \frac{1}{K_2} \right)^{-1}. \tag{1}$$

After a driving distance D_1, the mover translates over a distance δ (i.e., the clearance between the mover and stopper) with respect to platform M, and it contacts the stopper. The corresponding displacement X_1 of the output platform can be calculated from the relationship:

$$K_1(D_1 - X_1) = K_2 X_1 \tag{2}$$

which gives

$$X_1 = \frac{K_1}{K_1 + K_2} D_1. \tag{3}$$

Then, if the actuation continues in the forward direction, only the bearing K_2 will be deformed since the deformation of bearing K_1 is constrained by the forward stopper. Hence, the overall stiffness of the mechanism becomes:

$$K_{\text{range2}} = K_2. \tag{4}$$

Suppose that a maximal driving distance D_2 is produced by the actuator after the mover contacts the forward stopper. The overall output displacement of platform M can be calculated:

$$X_2 = X_1 + D_2 = \frac{K_1}{K_1 + K_2} D_1 + D_2. \tag{5}$$

Thus, the one-sided forward motion range of platform M is divided into two ranges of [0, X_1] and [X_1, X_2], which are assumed to be smaller and larger ranges, respectively.

Similarly, the backward motion range of the output platform is divided into two intervals by the backward stopper. In the two ranges, the stiffnesses of the system are different. The stage behaves as a variable stiffness mechanism.

B. Dual-Resolution Compliant Stage Design

Based on the foregoing design, the deformation of the mechanism is only attributed to K_2 in the larger motion range of [X_1, X_2]. Whereas in the smaller range of [0, X_1], the deformation is contributed by both bearings. The

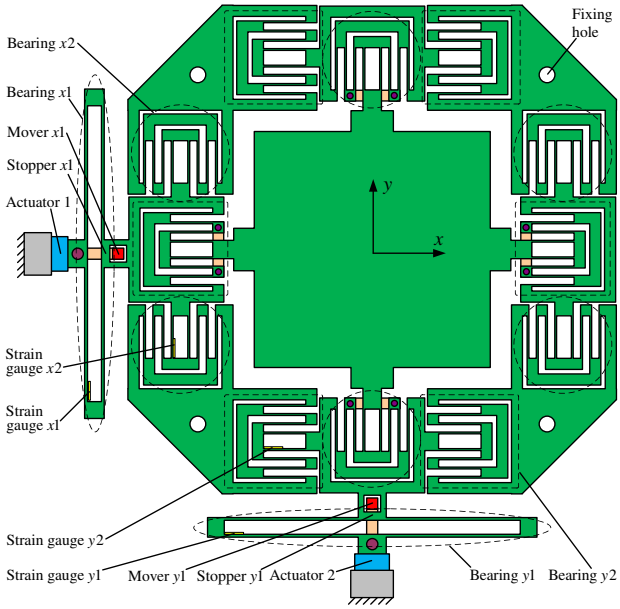

Fig. 2. Schematic diagram of a compliant XY micropositioning stage with dual-range and dual-resolution.

deformations Δ_1 and Δ_2 of the two compliant bearings are related by:

$$K_1 \Delta_1 = K_2 \Delta_2 \tag{6}$$

which describes the common actuation force.

Assume that $K_1 < K_2$, then it is deduced from (6) that $\Delta_1 > \Delta_2$, i.e., the deformation of bearing K_1 is greater than that of bearing K_2.

It is known that strain sensors (e.g., strain gauge, piezoresistive sensor) can be employed to measure the displacement of compliant mechanism indirectly by detecting the varying strain of deformed material. If the same type of strain sensor is adopted to measure two different deformations, the larger the deformation, the larger the output signal. That is, a larger deformation leads to a higher signal-to-noise ratio (SNR), i.e., higher measurement resolution.

Thus, using strain sensors, the deformation of bearing K_1 can be monitored with a higher positioning resolution in smaller motion range, and the deformation of bearing K_2 can be measured with a lower resolution in the larger range. By this, a micropositioning stage with dual-range and dual-resolution is devised. Specifically, the higher and lower resolutions are generated in the smaller and larger motion ranges, respectively.

III. Mechanical Design of a Compliant XY Micropositioning Stage

A dual-range, dual-resolution XY micropositioning stage is designed as an illustration, which is shown in Fig. 2. The leaf springs are adopted to obtain a large motion range of the compliant stage.

The x-axis motion is guided by bearings $x1$ and $x2$, while y-axis motion is produced by bearings $y1$ and $y2$. Owing to a symmetric design, the positioning in x and y directions

follow the same principle. The mover $x1$ is connected to the driving end of actuator #1, and stopper $x1$ is formed by a hole in the output platform. The bidirectional translations of mover $x1$ are restricted by stopper $x1$.

Besides, the bearings $x2$ and $y2$ form a decoupled XY stage, which ensures that the translational motion in x (y) direction is independent of that in y (x) direction. As compared with existing work [13], the XY stage exhibits a modified fixing scheme along with added bearings $x1$ and $x2$ to achieve the current objective.

A. Stiffness Calculation

The equivalent stiffnesses of the two guiding bearings in each working axis are calculated first. The bearing $x1$ consists of four fixed-guided flexures, which experience the identical deformations due to the identical dimensions. The equivalent stiffness can be derived as follows [13].

$$K_1 = \frac{Ebh_1^3}{l_1^3} \tag{7}$$

where E is the Young's modulus of the material; b, h_1, and l_1 represent the width, thickness, and length of the leaf flexures, respectively.

Considering that the bearing $x2$ is composed of six basic modules of compound parallelogram flexure, its stiffness can be calculated below [13].

$$K_2 = \frac{3Ebh_2^3}{l_2^3} \tag{8}$$

where h_2 and l_2 describe the thickness and length of the leaf flexures, respectively.

B. Motion Range Determination

Assume that the two motion ranges in each working axis are [0, $|R_1|$] and [$|R_1|$, $|R_1+R_2|$], respectively. To determine the relationship between motion range R_1 and clearance δ, the absolute deflection of bearing K_1 is derived as follows.

$$\delta = D_1 - R_1 \tag{9}$$

where D_1 is the driving displacement of the actuator.

Taking into account (3), the following equation holds.

$$D_1 = \frac{K_1 + K_2}{K_1} R_1 \tag{10}$$

Then, substituting (10) into (9), a fundamental operation gives

$$R_1 = \frac{K_1}{K_2}\delta \tag{11}$$

which means that the smaller range R_1 is governed by the clearance δ as well as the stiffnesses K_1 and K_2 of the two bearings. Thus, to generate a smaller motion range R_1, the clearance between mechanical mover and each stopper should be designed as:

$$\delta = \frac{K_2}{K_1} R_1. \tag{12}$$

The required input displacement from the actuator can be obtained from (10):

$$D_1 = (1 + \frac{K_2}{K_1})R_1. \tag{13}$$

Meanwhile, to avoid plastic deformation of the flexures, the stress experienced by bearing #1 due to a deflection δ should stay less than the yield stress σ_y of the material. Hence, the allowable maximum clearance can be computed:

$$\delta^{\text{allow}} = \frac{2\sigma_y l_1^2}{3Eh_1}. \tag{14}$$

To ensure the safety of the material, the one-sided smaller range should be designed to satisfy:

$$R_1 \le \frac{K_1}{K_2}\delta^{\text{allow}} = \frac{2\sigma_y l_1^2 K_1}{3Eh_1 K_2}. \tag{15}$$

As for the larger motion interval R_2, considering that only bearing $x2$ is deformed, the required input displacement from the actuator is derived as:

$$D_2 = R_2. \tag{16}$$

Similarly, to guarantee the safety of the material, the maximum allowable motion range of bearing $x2$ can be calculated:

$$\Delta_2^{\text{allow}} = \frac{4\sigma_y l_2^2}{3Eh_2}. \tag{17}$$

Therefore, to guarantee the safety of the material, the larger motion range should be designed to meet the condition:

$$R_2 \le \Delta_2^{\text{allow}} - R_1 = \frac{4\sigma_y l_2^2}{3Eh_2} - R_1. \tag{18}$$

C. Motor Stroke and Driving Force Determination

In this research, the voice coil motor (VCM) is employed to create a relatively large motion range. In order to produce an entire motion range of $R_1 + R_2$, a driving displacement of $D_1 + D_2 = (1 + \frac{K_2}{K_1})R_1 + R_2$ is needed, which should not exceed the stroke D_{stroke} of the actuator:

$$D_{\text{total}} = (1 + \frac{K_2}{K_1})R_1 + R_2 \le D_{\text{stroke}}. \tag{19}$$

Additionally, the stiffness of the stage should be sufficiently low so that it is able to be actuated by the VCM. Assume that $K_1 < K_2$, then it is derived from (1) and (4) that $K_{\text{range1}} < K_{\text{range2}}$, i.e., the stiffness in smaller motion range is lower than that in larger range. Thus, it is deduced that the maximum driving force σ_y occurs when the output platform arrives at the extremum of larger motion range. The required maximum driving force is calculated as follows.

$$F_{\max} = K_{\text{range2}}(R_1 + R_2) \le F_{\text{actuator}} \tag{20}$$

Substituting (4) and (8) into (20) yields

$$F_{\max} = \frac{Ebh_2^3}{l_2^3}(R_1 + R_2) \le F_{\text{actuator}} \tag{21}$$

which provides a guideline for the stage parameter design.

D. Sensor Design

Two sets of strain gauges are employed to measure the displacements in the smaller and larger motion ranges of the compliant stage. To enhance the signal-to-noise ratio (SNR), the strain gauges are glued around the maximum-stress positions of the leaf flexures related to bearings $x1$ ($y1$) and $x2$ ($y2$), respectively, as depicted in Fig. 2.

The relationship (6) indicates that $\frac{\Delta_1}{\Delta_2} = \frac{K_2}{K_1}$. By selecting $K_1 < K_2$, the relation of $\Delta_1 > \Delta_2$ is obtained. Hence, in the smaller motion range, the length change value of strain gauge $x1$ ($y1$) is larger than that of gauge $x2$ ($y2$). Therefore, a higher SNR is expected for the gauge $x1$ ($y1$). It follows that gauge $x1$ ($y1$) achieves a better measurement resolution than gauge $x2$ ($y2$).

Without loss of generation, assume that the stage output displacement is measured by the strain gauge sensors through quarter-Wheatstone bridge circuits. The bridge output voltage can be approximated as:

$$V_o = \frac{V_s}{4R} \times dR \tag{22}$$

where dR and R represent the change value and nominal value of the gauge resistance.

The gauge factor is expressed as:

$$S = \frac{dR/R}{\varepsilon} \tag{23}$$

where ε is the corresponding strain induced by the deformation of the flexure bearing. The strain ε is related to the experienced stress σ by:

$$\sigma = E\,\varepsilon \tag{24}$$

where E is the Young's modulus of the material.

Moreover, the relationship between the stress σ and guided deflection μ of a leaf flexure can be derived as:

$$\sigma = \frac{Khl\mu}{4I} \tag{25}$$

where $K = Ebh^3/l^3$ is the stiffness and $I = bh^3/12$ is the moment of inertia of a leaf flexure.

In view of the aforementioned equations, the relationship between the circuit output voltage V_o and the flexure deflection can be derived:

$$\mu = \frac{4l^2 V_o}{3hSV_s}. \tag{26}$$

It is noticeable that the deflections of flexures (μ_1 and μ_2) in bearing #1 and #2 are one-half and one-quarter of the entire translation (Δ_1 and Δ_2) of the bearing, respectively. In view of (6), the ratio of output voltages of the two strain gauges is obtained below:

$$\frac{V_{o1}}{V_{o2}} = \frac{2h_1 l_2^2 K_2}{h_2 l_1^2 K_1}. \tag{27}$$

In the following section, a dual-range, dual-resolution XY compliant stage is devised to illustrate the proposed design procedures.

TABLE I
MAIN PARAMETERS OF AN XY MICROPOSITIONING STAGE

Parameter	h_1	l_1	h_2	l_2	b	δ
Value (mm)	0.5	40	0.35	21	10	1.5

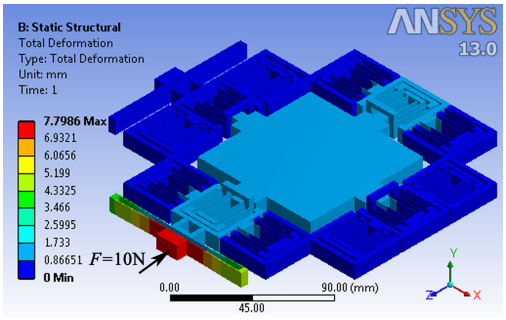

Fig. 3. Deformation result of static FEA simulation.

IV. CASE STUDY

As a case study, an XY micropositioning stage is designed to produce the smaller and larger motion ranges of R_1 = 0.2 mm and R_2 = 2.0 mm, respectively. The VCM provides the stroke of ±5 mm and maximum driving force of 29.2 N. Table I shows the stage parameters, which allow the generation of R_1^{allow} = 2.10 mm, R_2^{allow} = 11.79 mm, D_{total} = 8.02 mm, and $F_{\max}$ = 22.0 N, all satisfying the design guidelines. In addition, the designed parameters lead to the output voltage ratio of $\frac{V_{o1}}{V_{o2}}$ = 5.60. Therefore, the relationship of SNR of the two strain gauge sensors can be derived as $\frac{\text{SNR}_1}{\text{SNR}_2}$ = 5.60. It means that the resolution in smaller range has been improved by 5.60 times as compared with that in larger motion range.

A. FEA Simulation Results

To verify the static performance of the designed stage, static structural FEA simulations are carried out by applying an input force to produce the smaller and larger motions, respectively. For the smaller range, the deformation result of FEA simulation is illustrated in Fig. 3. To generate a motion range of ±0.2 mm, the required driving displacement is ±1.80 mm. Taking the FEA result as the benchmark, it can be seen that the analytical model result (±1.71 mm) is 5.0% lower than that of FEA. Moreover, simulation results reveal that the maximum translational range of each flexure in bearing $x1$ is ±2.02 mm. The discrepancy between the analytical model and FEA is only 0.5%.

Concerning the larger motion range, FEA results indicate that the maximum deflection of each flexure of bearing $x2$ is ±12.10 mm. As compared with FEA result, the analytical model underestimates the larger motion range by 2.6%. In order to generate a total motion range of ±2.2 mm, the FEA predicts that the required maximum driving force is 24.2 N. The difference between the analytical and FEA results is 9%.

The above discrepancies are all less than 10%, which mainly come from the assumption for the analytical models by considering the bending deformations of the leaf flexures

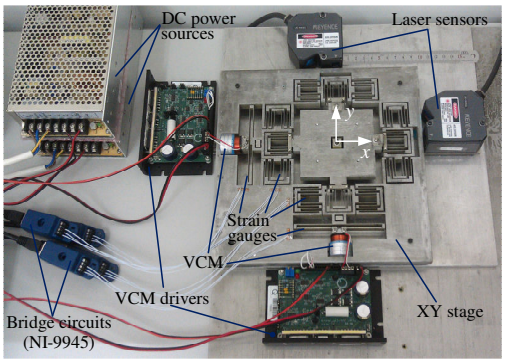

Fig. 4. A prototype of the XY micropositioning stage.

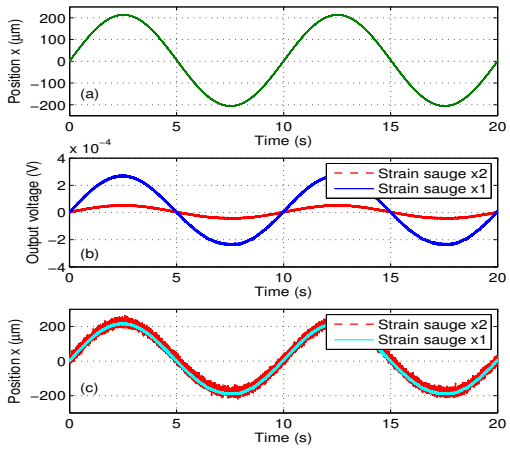

Fig. 5. (a) Output position measured by laser sensor; (b) voltage outputs of two strain gauge sensors; (c) position output of calibrated strain sensors.

only. The model accuracy can be enhanced by making use of the nonlinear modeling.

B. Dynamic Analysis Results

The modal analysis is performed to evaluate the dynamic performance of the stage. The first-two modes represent the translations along the x- and y-axes with similar resonant frequencies of 35.2 and 35.3 Hz, respectively. The third resonant mode at 72.5 Hz is attributed to the in-plane rotation of the stage output platform. It is found that the third resonant frequency is more than twice higher than the first-two fundamental frequencies, which indicates robust translations in the two working axes.

V. Prototype Development and Experimental Study

In this section, a prototype XY micropositioning stage is developed and its performance is verified through experimental studies.

A. Prototype Development

Fig. 4 shows a prototype XY stage which is fabricated from Al-7075 alloy by the wire-electrical discharge machining process. The stage possesses a dimension of 240 mm $\times$ 240 mm $\times$ 10 mm. Two VCMs (model: NCC04-10-005-1A, from H2W Techniques, Inc.) are selected to provide the maximum output force of 29.2 N and stroke of 10.2 mm. Each VCM is driven by the NI-9263 analogy output module through a VCM driver. The stage output displacements in the smaller and large range are measured by strain gauges, respectively. The strain gauges have a gauge factor of 2 and nominal resistance of 350 Ω.

To measure the quarter-bridge circuit output, the NI-9945 quarter bridge completion accessory is used to complete the 350 Ω sensor. The bridge output is acquired by using the NI-9237 bridge input module, which provides a high resolution of 24 bits. It can acquire the quarter-bridge signal directly and produce a maximum voltage output of $\pm$25 mV per volt of excitation voltage. For the calibration of the strain sensors, two Keyence laser displacement sensors are employed, which provide a resolution of 25 nm within the measurement range of 20 mm. In addition, an NI cRIO-9022 real-time controller combined with NI-9118 chassis is adopted to implement the controller. LabVIEW software is employed to implement a deterministic real-time control of the micropositioning system with a sampling rate of 5 kHz.

B. Experimental Studies and Results

The static performances of the XY stage in both x- and y-axes have been tested. Due to the similarity of the results for the two axes, only the x-axis results are presented.

First, the two strain sensors are calibrated. By applying a 0.1-Hz sinusoidal voltage signal with amplitude of 0.5 V to the driver of VCM #1, the stage output position in x-axis is measured by the laser sensor as shown in Fig. 5(a). The output voltages of the two strain gauges are depicted in Fig. 5(b). The strain gauge sensors are calibrated by comparing their output voltages to the laser sensor output. The outputs of the calibrated sensors are shown in Fig. 5(c), which exhibits obviously that the output of sensor $x2$ is noisier than that of sensor $x1$.

To quantify the resolutions of the two strain sensors, noise analysis is carried out. In this work, the noise mainly comes from the electric noise of the digital to analog converter. With zero voltage input, the noises of the two strain sensors have been recorded. It is found that the noises follow normal distributions closely with standard deviations (σ) of 1.625 μm and 8.517 μm, respectively. In order to quantify the noise level, the σ value is adopted as the sensor resolution [14]. Then, the resolution ratio of the coarse and fine sensors is derived as 5.24, i.e., the resolution in the smaller stroke has been improved by 5.24 times as compared with that in larger motion stroke. It is found that the experimental result is 6.4% lower than the analytical prediction of 5.6. This discrepancy mainly arises from the fabrication errors of the stage parameters, assembly errors of the VCM, and installation errors of the strain gauges.

Second, the magnitude of the two motion ranges are tested by applying a sinusoidal signal as shown in Fig. 6(a). The output position measured by the two strain sensors are plotted in Fig. 6(b). It is found that sensor $x1$ saturates in the limits of the range [–220 μm, 310 μm], which represents

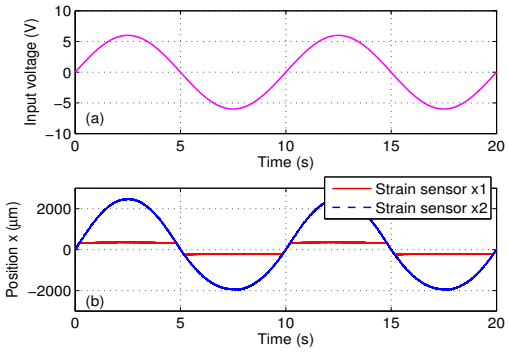

Fig. 6. (a) Input voltage; (b) output position obtained by two strain sensors.

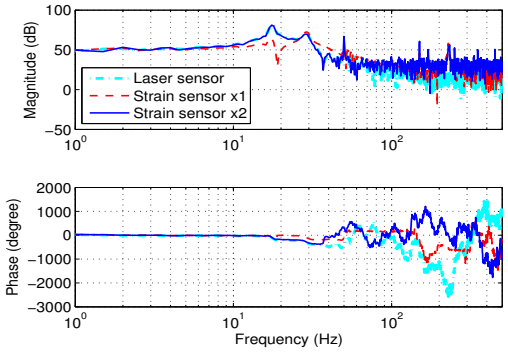

Fig. 7. Bode diagrams of frequency responses of the XY stage in x-axis.

the smaller motion range of the stage. In the larger range of [–1940 μm, -220 μm] and [310 μm, 2470 μm], the output displacement is measured by sensor $x2$ alone. The switch between the fine and coarse positioning can be realized by monitoring the output displacements. It is found that the smaller stroke is larger than the design objective of ± 0.2 mm. In addition, the overall motion range [–1940 μm, 2470 μm] is slightly larger than the design specification of 4.4 mm. Besides, the fact that both smaller and larger bidirectional motion ranges are not exactly symmetric with respect to zero is attributed to the manufacturing errors and the unequal clearance between the mover and each side of the limiter.

Third, the dynamic performance of the stage is examined by the frequency response method. Specifically, a swept-sine signal with the amplitude of 0.03 V and frequency range of 1–500 Hz is applied to drive the VCM #1. The frequency responses of the stage position output are shown in Fig. 7. It is observed that all of the three sensors predict the first resonant frequency at 17.5 Hz. However, the experimental result is lower than that assessed by FEA simulation. The discrepancy mainly comes from the added mass of the mover and moving coil of VCM, which is not considered in FEA simulation. The resonant frequency can be enhanced by reducing the mass of moving components, e.g., using a hollow structure.

It is found that the fine resolution of 1.625 μm can only be achieved in the smaller range around the home position of the stage. Besides, in the limits of smaller range, a rapid impact of the mover with stoppers may cause vibration of the flexure. As shown in the experimental results (see Fig. 6(b)), the impact can be eliminated by commanding a lower speed of the stage at the two limits. Other performance of the stage will be tested in future studies.

VI. Conclusion

The design and verification of a new XY compliant micropositioning stage with dual ranges and dual resolutions has been presented in this paper. Based on the concept of variable stiffness, a flexure-based stage is devised as an example. Analytical models have been established to predict the motion ranges, coarse/fine resolution ratio as well as driving force and stroke of the actuator, which have been verified by finite element analysis and experimental studies. Results show that the single-drive stage is capable of producing dual motion ranges in each working axis and the same type of strain gauge sensors is able to provide the fine and coarse resolutions in the small and large ranges, respectively.

References

[1] Y. Michellod, P. Mullhaupt, and D. Gillet, "Strategy for the control of a dual-stage nano-positioning system with a single metrology," in *Proc. of IEEE Conf. on Robotics, Automation and Mechatronics*, 2006, pp. 1–8.

[2] L. Chassagne, M. Wakim, S. Xu, S. Topcu, P. Ruaux, P. Juncar, and Y. Alayli, "A 2D nano-positioning system with sub-nanometric repeatability over the millimetre displacement range," *Meas. Sci. Technol.*, vol. 18, no. 11, pp. 3267–3272, 2007.

[3] E. S. Buice, D. Otten, R. H. Yang, S. T. Smith, R. J. Hocken, and D. L. Trumper, "Design evaluation of a single-axis precision controlled positioning stage," *Precis. Eng.*, vol. 33, no. 4, pp. 418–424, 2009.

[4] S. A. Zirbel, Q. T. Aten, M. Easter, B. D. Jensen, and L. L. Howell, "Compliant constant-force micro-mechanism for enabling dual-stage motion," in *Proc. of ASM Int. Design Engineering and Technical Conf*, 2012, pp. 191–198.

[5] J. P. Yang, G. K. Lau, C. P. Tan, N. B. Chong, B. Thubthimthong, and Z. M. He, "An electro-thermal micro-actuator based on polymer composite for application to dual-stage positioning systems of hard disk drives," *Sens. Actuator A-Phys.*, vol. 187, pp. 98–104, 2012.

[6] W. Dong, L. Sun, and Z. Du, "Design of a precision compliant parallel positioner driven by dual piezoelectric actuators," *Sens. Actuator A-Phys.*, vol. 135, no. 1, pp. 250–256, 2007.

[7] Q. Xu, "Design and development of a flexure-based dual-stage nanopositioning system with minimum interference behavior," *IEEE Trans. Automat. Sci. Eng.*, vol. 9, no. 3, pp. 554–563, 2012.

[8] T. J. Teo, I.-M. Chen, G. Yang, and W. Lin, "A flexure-based electromagnetic linear actuator," *Nanotechnology*, vol. 19, no. 31, p. 315501, 2008.

[9] M.-Y. Chen, T.-B. Lin, S.-K. Hung, and L.-C. Fu, "Design and experiment of a macro-micro planar maglev positioning system," *IEEE Trans. Ind. Electron.*, vol. 59, no. 11, pp. 4128–4139, 2012.

[10] Y. Song, J. Wang, K. Yang, W. Yin, and Y. Zhu, "A dual-stage control system for high-speed, ultra-precise linear motion," *Int. J. Adv. Manuf. Technol.*, vol. 48, pp. 633–643, 2010.

[11] S.-M. Suh, C. C. Chung, and S.-H. Lee, "Design and analysis of dual-stage servo system for high track density HDDs," *Microsyst. Technol.*, vol. 8, no. 2-3, pp. 161–168, 2002.

[12] A. Al Mamun, I. Mareels, T. H. Lee, and A. Tay, "Dual stage actuator control in hard disk-a review," in *Proc. of 29th Anual IEEE Conf. on Industrial Electronics Society*, 2003, pp. 2132–2137.

[13] Q. Xu, "New flexure parallel-kinematic micropositioning system with large workspace," *IEEE Trans. Robot.*, vol. 28, no. 2, pp. 478–491, 2012.

[14] J. Dong, S. M. Salapaka, and P. M. Ferreira, "Robust control of a parallel-kinematic nanopositioner," *J. Dyn. Sys., Meas., Control*, vol. 130, no. 4, p. 041007, 2008.